Biosynthesis of Hyperforin in *Hypericum perforatum*

Petra Adam,[†] Duilio Arigoni,[‡] Adelbert Bacher,[†] and Wolfgang Eisenreich*,[†]

Lehrstuhl für Organische Chemie und Biochemie, Technische Universität München, Lichtenbergstrasse 4, D-85747 Garching, Germany, and Laboratorium für Organische Chemie, Eidgenössische Technische Hochschule Zürich, HCI, CH-8093 Zürich, Switzerland

Cut sprouts of *Hypericum perforatum* were proffered solutions containing [1-^{13}C]glucose or [U-^{13}C$_6$]glucose. Hyperforin was isolated and analyzed by quantitative NMR spectroscopy. The labeling patterns show that the biosynthesis of hyperforin involves five isoprenoid moieties, which are derived entirely or predominantly (>98%) via the deoxyxylulose phosphate pathway. The phloroglucinol moiety is generated via a polyketide type mechanism.

Introduction

Hyperforin (**1**, Figure 1) is accumulated in amounts up to 5% (dry weight) in the flowers and leaves of St. John's wort, *Hypericum perforatum.*[1] Extracts of *Hypericum* are used widely to alleviate mild depression.[2] The antidepressant activity has been attributed to inhibition of various neurotransmitter receptors by hyperforin.[3−6] Hyperforin has also been shown to display antibacterial[7] and cytostatic activity.[8] On the basis of the reports on inhibition of multidrug resistant *Staphyloccoccus aureus,*[9] the compound has attracted renewed interest as an antibacterial agent.

Recent studies have addressed certain risks involved in the widespread use of *H. perforatum* as an herbal medicine. Hyperforin and other compounds of the plant can decrease the blood levels of important drugs such as cyclosporin, human immunodeficiency virus (HIV) protease inhibitors, cytostatic compounds, anticoagulants, oral antidiabetics, and contraceptives via enhanced metabolic degradation attributed to increased expression of cytochrome P$_{450}$ enzymes involved in the detoxification of the lipophilic organic compounds.[10−12] Thus, the efficacy of therapy with life-saving drugs such as cyclosporin or HIV inhibitors may be jeopardized by the adjuvant therapy (prescribed or self-administered) with the herbal medicine. These findings were hailed as a "breakthrough of the year 2000" by *Science.*[13]

Hyperforin (**1**, Figure 1) is a bicyclic compound[14−16] whose biosynthesis is still unknown. The structure suggests a meroterpenoid origin.[14] Recent studies have shown a wide variety of plant terpenoids to be formed by a nonmevalonate pathway via 1-deoxy-D-xylulose 5-phosphate (**5**) (Figure 2) (for review, see ref 17).

This paper shows that the biosynthesis of hyperforin involves five isoprenoid moieties, which are derived predominantly (>98%) via the nonmevalonate pathway. The acyl phloroglucinol moiety is generated via a polyketide type mechanism; a scheme is suggested for its subsequent transformation into **1**.
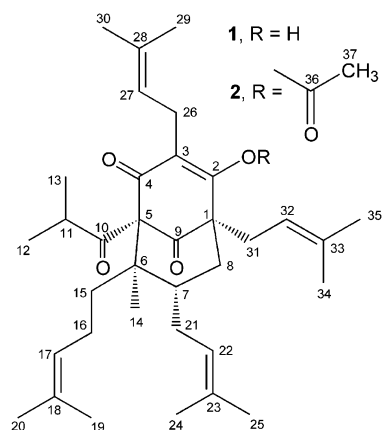
---

* To whom correspondence should be addressed. Tel: +49-89-289-13043. Fax: +49-89-289-13363. E-mail: wolfgang.eisenreich@ch.tum.de.
  † Technische Universität München.
  ‡ Eidgenössische Technische Hochschule Zürich.

Figure 1. Structures of **1** and **2**.

Results

Cut sprouts of *H. perforatum* were immersed into a solution containing 1% (w/w) [1-^{13}C]glucose or 0.05% [U-^{13}C$_6$]glucose (99.9% ^{13}C enrichment) and 0.95% (w/w) unlabeled glucose. The samples were incubated in the dark for 2 weeks. Hyperforin (about 100 mg) was isolated from the plant material (fresh weight, 25 g) and analyzed by NMR spectroscopy. Because the NMR spectrum of **1** displays broadened signals for C-1, C-2, C-4, C-5, and C-8, the biosynthetic hyperforin was converted into the 2-acetyl derivative **2** (Figure 1), which gave sharp NMR signals for all carbon atoms.
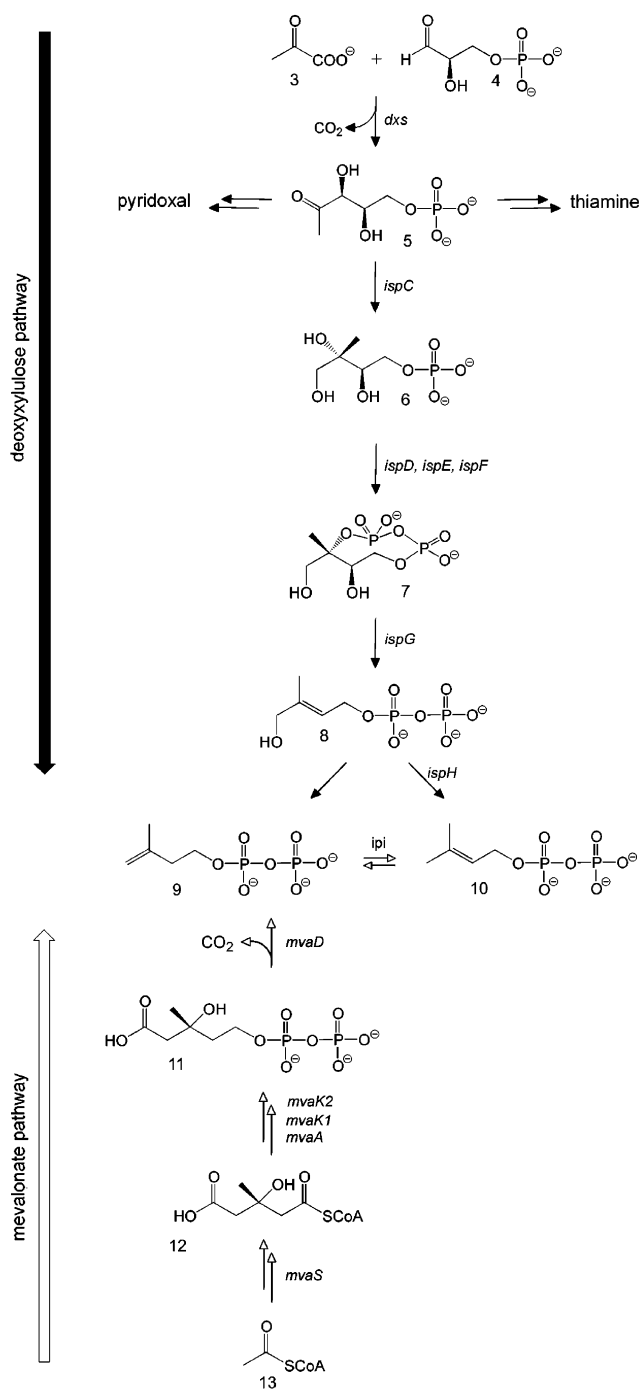
As a prerequisite for biosynthetic studies by ^{13}C NMR spectroscopy, all ^{13}C NMR signals of the target molecules must be assigned. Only partial NMR assignments for hyperforin were available from the literature.[18,19] NMR signals of **2** had not been assigned previously to the best of our knowledge. Therefore, all ^{1}H and ^{13}C NMR signals of **1** and **2** were assigned unequivocally by one- and two-dimensional NMR experiments (see Supporting Information).

Quantitative NMR analysis (for details, see Experimental Section) of **1** and **2** from the experiment with [U-^{13}C$_6$]glucose showed that the average ^{13}C abundance of all hyperforin carbon atoms of **1** and **2** (Table 1) was 1.8 ± 0.3% corresponding to a ^{13}C excess of 0.7 ± 0.3%. From the molar fraction of ^{13}C-labeled glucose in the proffered solution (about 5%), a specific incorporation

Figure 2. Deoxyxylulose phosphate pathway and the mevalonate pathway of isopentenyl diphosphate (**9**) and dimethylallyl diphosphate (**10**) biosynthesis.

rate of $14 \pm 6\%$ can be calculated. Assuming that unlabeled CO_2 was not fixed to a significant extent during the feeding experiment in the dark, this means that $86 \pm 6\%$ of the recovered hyperforin was already present in the cut sprouts at the beginning of the experiment.

Most ^{13}C signals of **1** and **2** from the experiment with [U-13C6]glucose showed satellite signals due to [13]C−[13]C coupling indicative of the presence of multiple ^{13}C-labeled isotopomers. The relative intensities of the satellite signals were well above those characteristic of the natural abundance background (1.1% for each adjacent ^{13}C atom in natural abundance material).

Table 1. [13]C Abundances and Relative Fractions of Multiple ^{13}C-Labeled Isotopomers in **1** and the **2** Obtained from Cut Sprouts of *Hypericum perforatum* Immersed into Solutions Containing [1-13C]Glucose or [U-13C6]Glucose

	precursor					
	[1-13C]glucose		[U-13C6]glucose			
	% [13]C		% [13]C[a]		% [13]C[13]C[b]	
position	1	2	1	2	1	2
1	nd	2.7	nd	2.2	nd	29.9 (2, 9)
2	nd	1.3	nd	1.8	nd	14.9 (3), 15.3 (1)
3	2.4	2.4	1.6	1.9	nd	16.9 (2), 16.3 (4)
4	nd	1.3	nd	2.0	nd	15.7 (2), 15.7 (3)
5	nd	2.5	nd	2.2	nd	29.6 (1, 9)
6	nd	1.0	nd	1.6	nd	28.1 (14)
7	1.1	1.1	1.5	1.3	23.3 (8)	23.6 (8)
8	2.8	2.0	nd	1.6	nd	28.9 (7)
9	1.2	1.3	1.8	2.2	31.4 (1,9)	31.1 (1, 9)
10	1.2	1.2	1.5	1.5		
11	1.0	1.1	nd	1.6	nd	31.5 (12)
12	2.0	1.9	1.5	1.4	23.7 (11)	22.0 (11)
13	2.0	2.0	1.5	1.3		
14	2.5	2.5	1.7	1.7	30.5 (6)	28.2 (6)
15	1.2	1.2	1.4	1.4		
16	2.2	2.3	1.6	1.7	10.1 (17), 24.9 (17, 20)	10.4 (17), 25.2 (17, 20)
17	1.2	1.1	1.8	1.7	8.4(16), 24.9 (16, 20)	7.8 (16), 25.2 (16, 20)
18	1.3	1.3	1.8	2.1	32.1 (19)	31.0 (19)
19	2.9	3.0	1.8	2.3	33.1 (18)	nd
20	1.5	1.3	1.7	1.7		
21	2.2	2.3	1.6	1.7	11.1(22), 24.3 (22, 25)	10.7 (22), 22.4 (22, 25)
22	1.1	1.1	1.8	1.7	10.2 (21), 23.7 (21, 25)	10.7 (21), 22.4 (21, 25)
23	1.2	1.4	1.8	2.3	33.0 (24)	33.2 (24)
24	2.8	2.7	1.8	nd	31.4 (23)	nd
25	1.4	1.4	1.7	1.7		
26	2.1	2.1	1.8	1.8	10.2 (27), 25.6 (27, 30)	10.4 (27), 25.2 (27, 30)
27	1.1	1.1	1.9	1.8	10.0 (26), 24.9 (26, 30)	10.4 (26), 25.6 (26, 30)
28	1.3	1.3	1.8	2.2	32.2 (30)	33.3 (30)
29	1.5	1.5	1.6	nd		
30	2.8	2.9	1.8	2.2	32.0 (28)	27.2 (28)
31	2.2	2.0	1.6	1.7	10.1 (32), 27.2 (32, 35)	8.8 (32), 24.5 (32, 35)
32	1.1	1.1	1.7	1.7	9.2 (31), 25.4 (31, 35)	8.8 (31), 24.5 (31, 35)
33	1.2	1.4	2.0	2.3	34.9 (34)	37.4 (34)
34	2.7	2.6	1.8	1.9	34.8 (33)	32.1 (33)
35	1.4	1.4	1.6	2.1		
36		1.2		1.4		
37		1.1		1.1		

[a] [13]C abundance. [b] Calculated as the fraction of the ^{13}C-coupled satellites in the global ^{13}C NMR intensity of a given atom. Coupling partners are in parentheses.

As examples, ^{13}C NMR signals for C-2 and C-4 of **2** are shown in Figure 3. The central signals represent [2-13C1]- and [4-13C1]-isotopomers, which are derived from unlabeled glucose or were already present in the sprouts prior to the labeling period. The C-2 signal displays two pairs of ^{13}C-coupled satellites, one of which is caused by ^{13}C coupling with C-3 (coupling constant, 79.0 Hz) reflecting a [2,3-13C2] isotopomer, and the other one is caused by ^{13}C coupling with C-1 (coupling constant, 47.6 Hz) reflecting the presence of a [1,2-13C2] isotopomer. Similarly, the signal for C-4 shows two satellite pairs representing [3,4-13C2]- and [4,5-13C2]-**2**. As a consequence of heavy isotope shift effects, the satellite pairs are not strictly symmetrical with respect to the central signal.

C-2   C-4
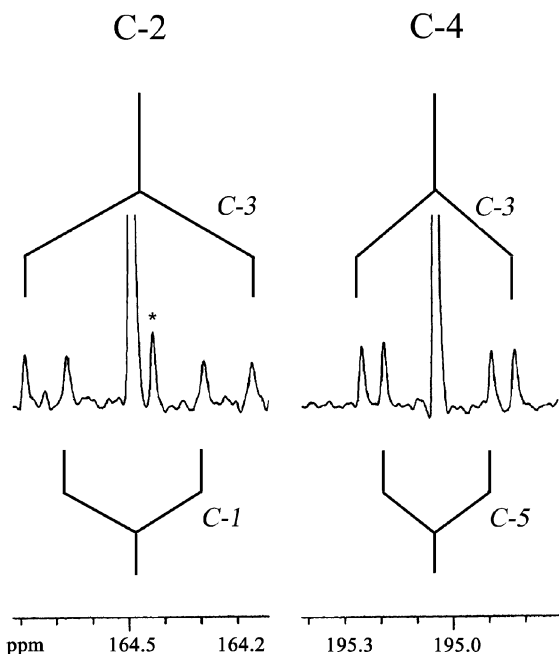
Figure 3. ^{13}C NMR signals for C-2 and C-4 of **2** obtained from the experiment with [U-[13]C$_6$]glucose. [13]C couplings are indicated. *, impurity.
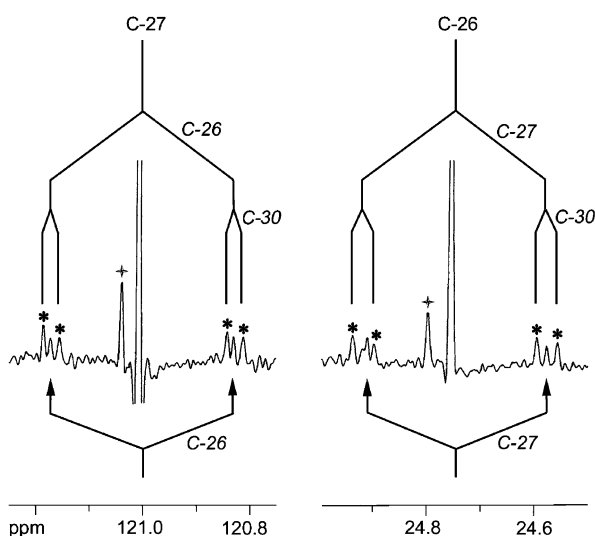
Figure 4. ^{13}C NMR signals for C-26 and C-27 of **2** obtained from the experiment with [U-[13]C$_6$]glucose. [13]C couplings are indicated. +, impurities.

The signal integrals of ^{13}C satellites attributed to multiply ^{13}C-labeled isotopomers afford the relative

amounts of the specific isotopomer by comparison with the overall signal intensity for a given carbon atom (Table 1). By multiplication of these values with the absolute ^{13}C abundance of the given atom position (cf. Table 1), the molar contribution of each respective isotopomer can be calculated. For example, the signal intensities of the satellite signals for [1,2-[13]C$_2$]- and [2,3-[13]C$_2$]-**2** were apparently identical (15.3 and 14.9% of the overall signal intensity for C-2, cf. Table 1). On the basis of the overall ^{13}C abundance of 1.8% for C-2, the molar contributions of [1,2-[13]C$_2$]- and [2,3-[13]C$_2$]-**2** were calculated as 0.28 and 0.30 mol %.

Some of the coupling satellites showed a fine structure caused by [13]C−[13]C coupling via two or three carbon bonds. For example, each of the signals for C-26 and C-27 showed six satellites (Figure 4). The central signals in each satellite pattern (indicated by arrows in Figure 4) had identical distances of 43.4 Hz implying coupling between the two respective atoms. The one bond coupling between C-26 and C-27 was also confirmed by the double quantum coherence of C-26/C-27 detected in the INADEQUATE experiment (cf. Figure 5). Therefore, the satellite pair indicated by arrows in Figure 4 was attributed to the presence of a [26,27-[13]C$_2$] isotopomer. The four satellite signals indicated by asterisks in Figure 4 were caused by simultaneous coupling of three ^{13}C atoms. On the basis of the coupling constants (i.e., one large coupling via one bond with a coupling constant of 43.4 Hz and one long-range coupling via two or three bonds with coupling constants of 3.3 and 4.6 Hz, respectively), these signals were assigned to [26,27,30-[13]C$_3$]-**2**.

The relative integrals of the satellite signals afforded relative abundances of the specific isotopomers (cf. Table 1), which could be converted into absolute isotopomer abundances (in mol %) on the basis of the overall ^{13}C abundances of C-26 (1.8%) and C-27 (1.8%). From the fact that quantitative information on isotopomer abundances can be gleaned from all NMR signals reflecting the specific isotopomers, averaged isotopomer contributions can be obtained (i.e., from the signals of C-26 and C-27 in the specific example). Thus, the abundances of [26,27-[13]C$_2$]-**2** and [26,27,30-[13]C$_3$]-**2** were 0.13 ± 0.02 and 0.38 ± 0.05 mol %, respectively. The low standard deviations show the accuracy of the quantitative analysis.

The abundances of 21 different multiply ^{13}C-labeled isotopomers are summarized in superimposed form in Figure 6A. Double-labeled isotopomers are indicated by
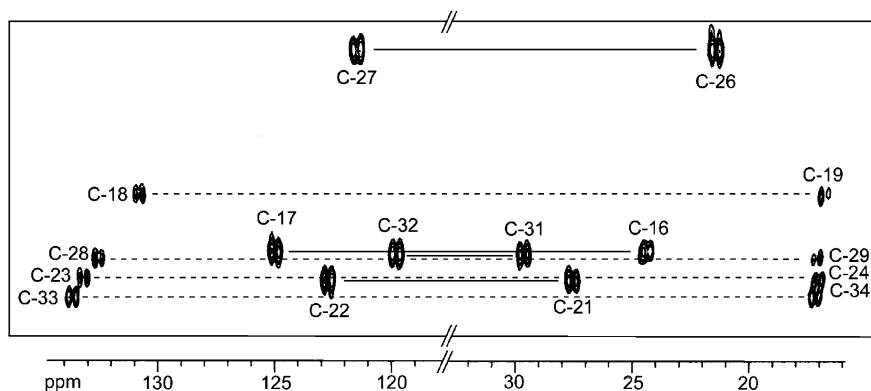
Figure 5. Part of a two-dimensional INADEQUATE spectrum of **2**.
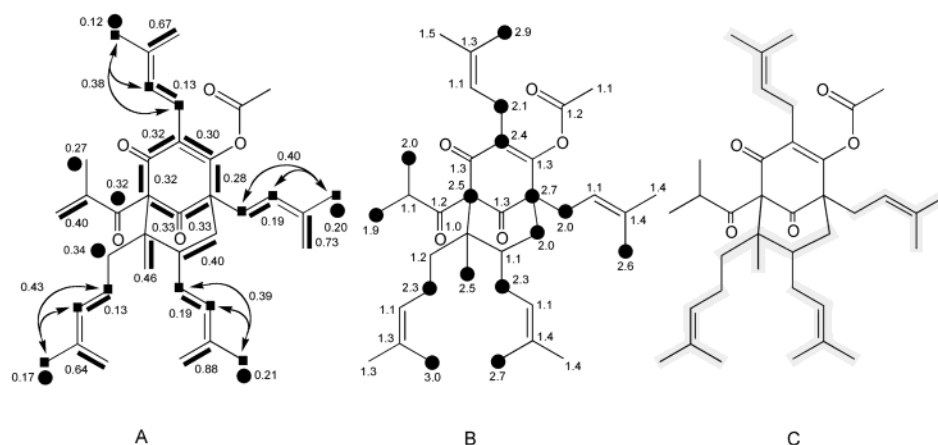
Figure 6. Isotopomer composition of **2** (A) from the experiment with [U-$^{13}C_6$]glucose. Bold lines indicate adjacent ^{13}C-labeled carbon atoms that were transferred from the same molecule of [U-$^{13}C_6$]glucose. Arrows connect three ^{13}C atoms (indicated by filled squares) that were transferred from the same molecule of [U-$^{13}C_6$]glucose. Filled dots represent $^{13}C_1$ isotopomers with ^{13}C abundances well above the natural abundance contributions (i.e., more than 1.2% ^{13}C abundance corresponding to more than 0.1% ^{13}C excess). Numbers indicate ^{13}C enrichments in mol %. (B) From the experiment with [1-^{13}C]glucose. Numbers indicate ^{13}C abundances. Filled dots indicate atoms with ^{13}C abundances higher than 1.9%. (C) Isoprenoid building blocks as derived from the isotopomer pattern are shaded.

bold lines connecting ^{13}C atoms within the same molecule. Triple-labeled isotopomers are shown as filled squares and arrows connecting ^{13}C atoms within the same molecule, and ^{13}C enrichments at single positions (i.e., with ^{13}C abundances above the natural abundance contribution of 1.1%) are symbolized by dots. The numbers indicate the ^{13}C enrichments of each respective isotopomer in mol %.

Six $^{13}C_2$ isotopomers with directly adjacent ^{13}C atoms were found in the phloroglucinol ring, and one $^{13}C_2$ isotopomer ([11,12-$^{13}C_2$]) was detected in the acyl side chain. Two $^{13}C_2$ isotopomers were observed in each of the three dimethylallyl moieties ([21,22-$^{13}C_2$], [23,24-$^{13}C_2$], [26,27-$^{13}C_2$], [28,29-$^{13}C_2$], [31,32-$^{13}C_2$], and [33,-34-$^{13}C_2$]). Moreover, long-range couplings via two or three carbon bonds demonstrated the presence of [26,-27,30-$^{13}C_3$], [21,22,25-$^{13}C_3$], and [31,32,35-$^{13}C_3$] isotopomers. The moiety of hyperforin comprising C-6 to C-8 and C-14 to C-20 showed four $^{13}C_2$ isotopomers, as well as one $^{13}C_3$ isotopomer (i.e., [16,17,20-$^{13}C_3$]) (Figure 6A).

A quantitative NMR analysis was also performed with **2** from the experiment with [1-^{13}C]glucose. As shown in Figure 7, the signal intensities for certain atoms were found to exceed the signal intensity of the methyl carbon of the acetyl side chain (C-37, derived from acetyl chloride with 1.1% ^{13}C abundance) by a factor of approximately 2. The ^{13}C abundances for other carbon atoms were calculated on the basis of the reference value of 1.1% for C-37. Fifteen carbon atoms of **2** had acquired ^{13}C with an average ^{13}C abundance of 2.4 ± 0.3% ^{13}C, whereas the remaining atoms had a ^{13}C abundance of 1.2 ± 0.1%, i.e., in the natural abundance range (Figure 6B).

Discussion

In earlier isotope perturbation experiments with ^{13}C-labeled glucose as precursor, we compared isotopomer compositions in target molecules (i.e., a given secondary metabolite) with isotopomer compositions in central metabolites (for example, acetyl-CoA, triose phosphate, and pyruvate), which were reconstructed from the
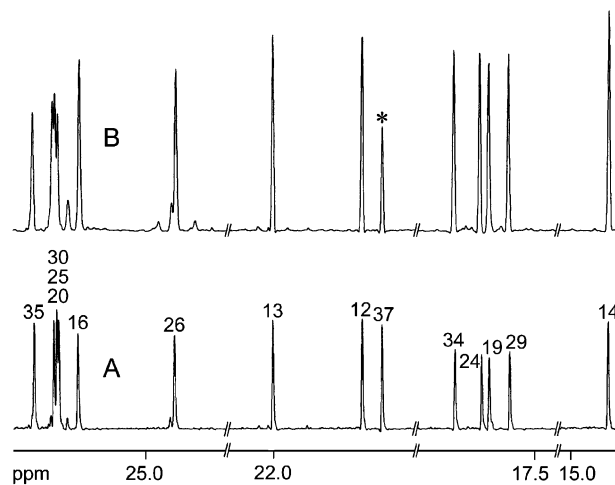

Figure 7. Part of ^{13}C NMR spectra of hyperforin (A) with natural ^{13}C abundance; (B) from the experiment with [1-^{13}C]glucose.

detected labeling patterns of amino acids and nucleosides by retrobiosynthetic analysis[20,21] (for review, see also refs 22 and 23). This approach could not be used in the present study since cut sprouts of *Hypericum* did not biosynthesize amino acids and nucleosides in sufficient amounts during the feeding period. However, the labeling patterns of hyperforin can be interpreted on the basis of the known utilization of exogenous glucose by plants.[20,24−27]

On the basis of utilization of exogenous glucose via the glycolytic pathway, glycogenesis, and the pentose phosphate pathway, labeling patterns can be predicted for potential terpenoid precursors, that is, acetyl-CoA (**13**) in the mevalonate pathway or pyruvate (**3**) and glyceraldehyde 3-phosphate (**4**) in the deoxyxylulose phosphate pathway (for review, see ref 23) (Figure 2). Thus, [U-$^{13}C_3$]-, [1-$^{13}C_1$]-, and [2,3-$^{13}C_2$]glyceraldehyde 3-phosphate (**4**) are formed from a mixture of [U-$^{13}C_6$]-glucose and unlabeled glucose by glycolysis and the reductive branch of the pentose phosphate cycle (Figure 8). Following the same mechanisms, [3-^{13}C]glyceralde-
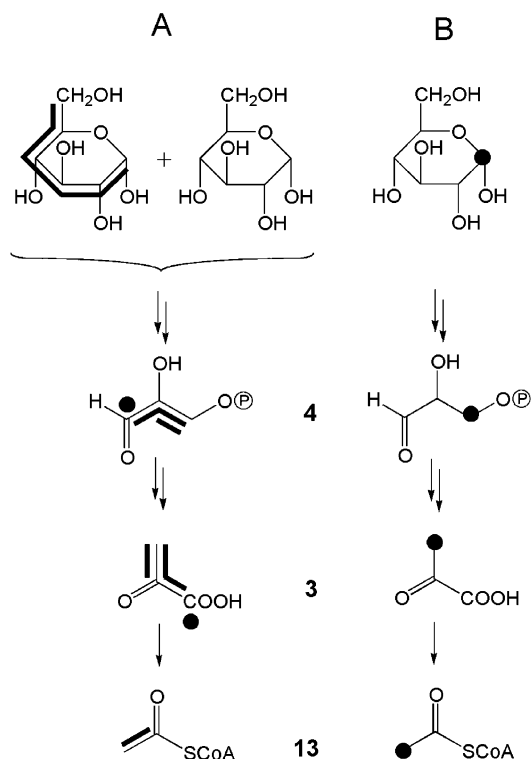
Figure 8. Isotopomer compositions of triose phosphate (**4**), pyruvate (**3**), and acetyl-CoA (**13**) predicted by reactions in the glycolysis and the pentose phosphate pathway. (A) Starting from a mixture of [U-^{13}C$_6$]glucose and glucose with natural ^{13}C abundance; (B) starting from [1-^{13}C]glucose. For other details, see legend to Figure 6.

hyde 3-phosphate is obtained from [1-^{13}C]glucose. Further downstream, these isotopomers afford [U-^{13}C$_3$]-, [1-^{13}C$_1$]-, and [2,3-^{13}C$_2$]pyruvate (**3**) from [U-^{13}C$_6$]glucose and [3-^{13}C]pyruvate from [1-^{13}C]glucose, respectively. Oxidative decarboxylation of pyruvate leads to [U-^{13}C$_2$]-acetyl-CoA (**13**) and to [2-^{13}C]acetyl-CoA in the experiments with [U-^{13}C$_6$]- and [1-^{13}C]glucose, respectively (Figure 8). With the labeling pattern of the early precursors of the terpenoid biosynthetic pathways at hand, the labeling patterns for DMAPP via the mevalonate and the nonmevalonate pathway can be predicted as indicated with panels B and C, respectively, in Figure 9. In each experiment, the labeling patterns of the three dimethyl allyl moieties were identical within the ex-

perimental limits (Figure 6A,B). Their averaged values, as indicated in Figure 9A, matched the pattern predicted for the nonmevalonate pathway (Figure 9C) but not that of the mevalonate pathway (Figure 9B).

The isotopomer compositions of five carbon atoms (i.e., C-16 to C-20) in the dimethylbutenyl side chain of hyperforin (Figure 6) were in agreement with the averaged labeling pattern of the dimethyl allyl side chains. We therefore concluded that these atoms were also derived from DMAPP via the deoxyxylulose phosphate pathway.

Finally, the labeling pattern for the five carbon unit comprising C-6, C-7, C-8, C-14, and C-15 of hyperforin also suggested an isoprenoid origin. As shown in Figure 6, the isotopomer composition in this unit closely resembled that of the dimethyl allyl moieties. The expected triple ^{13}C-labeled isotopomer was not observed, probably as a consequence of ^{13}C$-^{13}$C long-range coupling constants of C-7/C-8 and C-15 below the resolution limits. Even with this qualification, the labeling patterns were highly characteristic for an isoprenoid origin via the deoxyxylulose phosphate pathway. The isoprenoid building blocks incorporated into **1** are shown schematically in Figure 6C.

The isotopomer patterns detected for the acyl phloroglucinol moiety of hyperforin (Figure 6A,B) suggested a polyketide origin with isobutyryl-CoA (**17**) as a starter unit, which was subsequently lengthened by three malonyl-CoA units (**18**) (Figure 10). Cyclization of the linear precursor **19** would then lead to the acylphloroglucin **20**. As a consequence of unhindered rotation of the C2 symmetric aromatic ring of **20**, carbon atoms at the ortho and meta positions to the acyl group become pairwise stereohomotopic, and accordingly, signals with half of the normal intensity can be detected for six different ^{13}C$_2$ isotopomers carrying labels derived from the aromatic ring of the precursor in the NMR spectrum of **2** from the experiment with [U-^{13}C$_6$]glucose (Figure 6A).

The labeling pattern observed in the starter unit, isobutyryl-CoA (**17**), suggests its biosynthetic origin via metabolism of valine (**16**). More specifically, isobutyryl-CoA (**17**) could be formed from two units of pyruvate (**3**) via α-acetolactate (**14**) and a-ketoisovalerate (**15**). The labeling patterns detected for the acyl moiety in **2** perfectly matched the predictions shown in Figure 10.
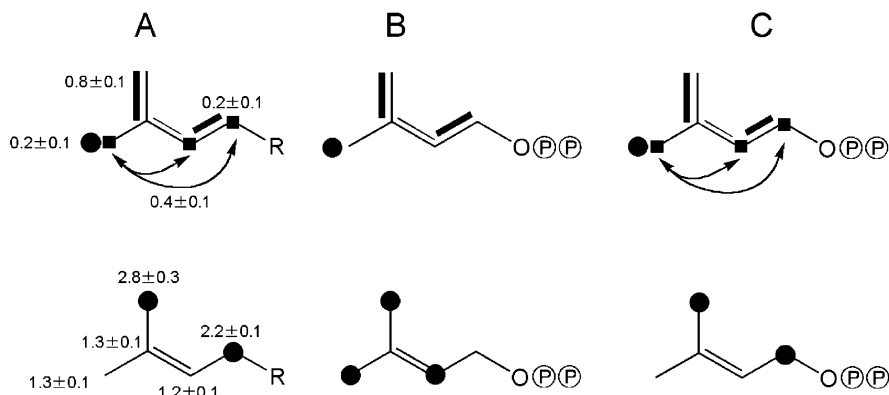
Figure 9. Isotopomer composition of the dimethylallyl moieties in hyperforin from the experiments with [U-^{13}C$_6$]glucose (top) and [1-^{13}C]glucose (bottom). (A) Averaged values from the data shown in Figure 6; (B) predicted via the mevalonate pathway of DMAPP biosynthesis; (C) predicted via the deoxyxylulose phosphate pathway of DMAPP biosynthesis. For other details, see legend to Figure 6.
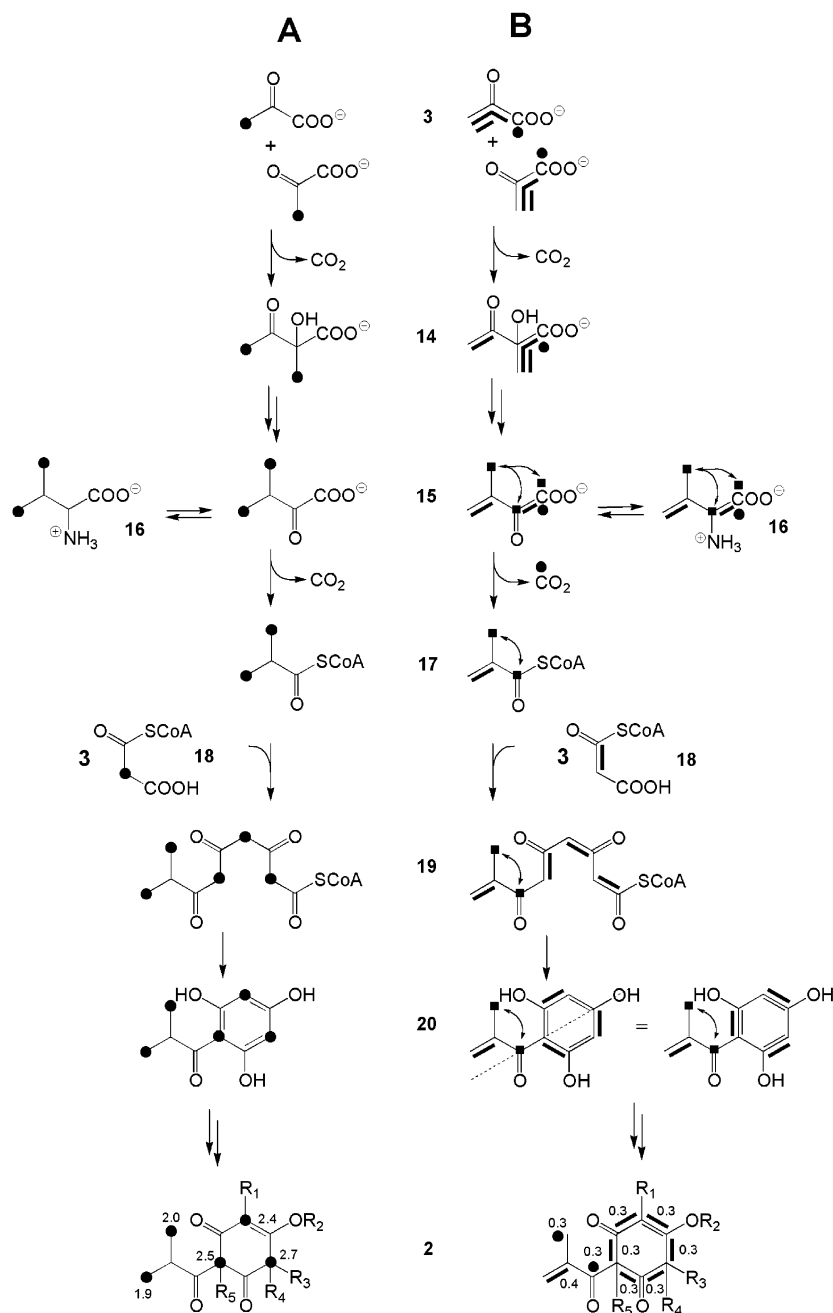
Figure 10. Isotopomer compositions of the acylphloroglucinol moiety in **2** from the experiments with [1-^{13}C]glucose (A) and [U-^{13}C$_6$]glucose (B). The isotopomer compositions of the putative precursors **17** and **20** are predicted by reactions of valine biosynthesis and polyketide metabolism, respectively. For other details, see legend to Figure 6.

Notably, the two diastereotopic methyl groups 12 and 13 of **2** displayed different labeling patterns in the experiment with [U-^{13}C$_6$]glucose. Thus, the signal of C-12 (δ 20.75 ppm) was characterized by intense coupling satellites due to coupling with C-11 (coupling constant, 34.1 Hz) whereas the signal of C-13 (δ 21.61 ppm) was a singlet. In keeping with the known stereochemical course of valine biosynthesis,[28] this singlet must be assigned to the pro-S methyl group in the acyl moiety of **2**.

The labeling patterns detected in this work shed some light on the mechanisms involved in the formation of the bicyclic ring system of **1**. Clearly, elaboration of **1** from the unsubstituted acylphloroglucinol precursor **20** requires a triple electrophilic substitution of the aromatic nucleus involving one geranyl pyrophosphate and

two DMAPP units as well as a ring closure triggered by electrophilic attack of a third DMAPP on the 2′/3′ double bond of the preimplanted geranyl chain. While the sequence of the necessary steps remains to a large extent unidentified, mechanistic considerations require that the cyclization be preceded by quaternization of the C atom to which the geranyl chain is appended, since subsequent quaternization of a preformed bicyclic intermediate would involve the participation of an unduly strained bridgehead enolate ion. One of the remaining possibilities satisfying this restriction and substantiating an earlier suggestion by Bystrov[14] is illustrated in Figure 11. The known stereochemistry of C-6 and C-7 in hyperforin[15,16] certifies that in the ring closure step an anti addition is taking place at the (E)-double bond of the immediate precursor (**22**).
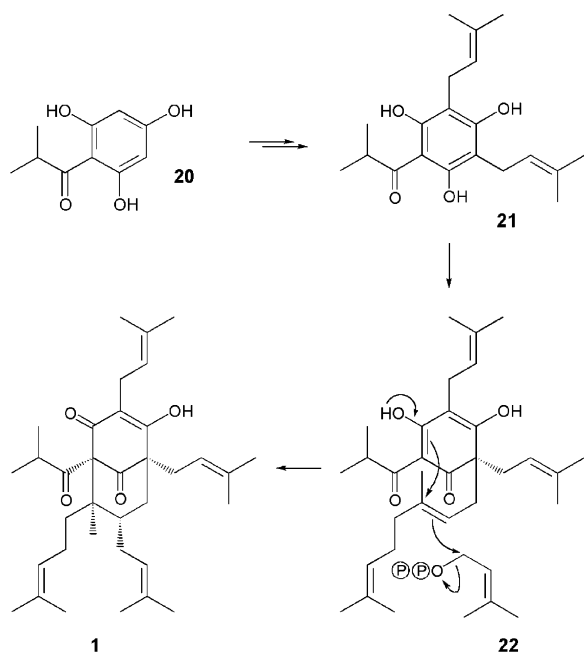
Figure 11. Hypothetical mechanism of hyperforin biosynthesis.

Experimental Section

Chemicals. [1-^{13}C]Glucose (99% ^{13}C enrichment) and [U-^{13}C$_6$]-glucose (99% ^{13}C enrichment) were obtained from Omicron, South Bend, Indiana.

Plant Material. Thirty 10 cm long sprouts of *H. perforatum* containing 5−10 young flower buds were cut from a wild *H. perforatum* plant and immediately immersed into a solution containing 1% (w/w) [1-^{13}C]glucose (99% ^{13}C enrichment). A second experiment was carried out with a solution containing 0.05% (w/w) [U-^{13}C]glucose (99% ^{13}C enrichment) and 0.95% (w/w) unlabeled glucose. The plant segments were incubated in the dark at 20 °C for 2 weeks. Small pieces were cut from the stems once per day.

Isolation of Hyperforin. All experiments were carried out in the dark, and all solvents were saturated with N$_2$. The plant material (fresh weight, 25 g) was triturated with liquid nitrogen. The cold slurry was transferred into a flask and extracted with 150 mL of *n*-heptane under a nitrogen atmosphere for 15 min. The slurry was filtered. The solution was concentrated to dryness under reduced pressure. The residue was dissolved in 100 mL of *n*-heptane, which had been saturated with methanol. The yellow solution was extracted three times with 50 mL of methanol saturated with *n*-heptane.[1] The alcoholic fractions were combined and concentrated to dryness under reduced pressure. The residue (120 mg) was applied to a column of silica gel (Silica Gel 60, Merck, Darmstadt, Germany, 20 × 1 cm), which was developed with a mixture of hexane and ethyl acetate (9:1; v/v). Aliquots were spotted on thin-layer chromatography (TLC) (Silica Gel 60 F$_{254}$, Merck), which was developed with the same solvent mixture. The TLC plates were dried and sprayed with a mixture of anisaldehyde/sulfuric acid/acetic acid (1:2:100; v/v). Hyperforin afforded a blue spot with an R_f value of 0.42. Fractions were combined and concentrated to dryness under reduced pressure (colorless oil, 95.8 mg). The purity was higher than 95%, as estimated from ^{1}H NMR.

Acetylation of Hyperforin. Hyperforin (40 mg) was dissolved in 1.2 mL of dry methylene chloride. The mixture was kept on ice. Triethylamin (150 μL) and 10 μL of acetyl chloride were added. The solution was stirred for 1 h. The reaction was stopped by adding 10 μL of water. The organic phase was dried over sodium sulfate and was concentrated under a stream of nitrogen. The crude product was applied to a column of Silica Gel 60 (10 × 1 cm, Merck), which was developed with a mixture of hexane and ethyl acetate (9:1; v/v).

The effluent was analyzed by TLC on silica gel 60 F$_{254}$ using a mixture of hexane and ethyl acetate (9:1; v/v) as solvent. The plates were dried and sprayed with a mixture of anisaldehyde/sulfuric acid/acetic acid (1:2:100; v/v). Acetylated hyperforin was detected as a green spot with an R_f value of 0.61. Fractions were combined and concentrated to dryness (colorless oil). Yield, 38 mg (89%). The purity was higher than 95%, as estimated from ^{1}H NMR.

NMR Spectroscopy. Compounds **1** or **2** were dissolved in CD$_3$OD. ^{1}H and ^{13}C NMR spectra were recorded at 500.13 and 125.76 MHz, respectively, using a Bruker DRX500 spectrometer at a temperature of 17 °C. The data were processed with standard Bruker software (XWINNMR 3.0). Two-dimensional COSY, NOESY, HMQC, and HMBC experiments were measured with standard Bruker parameters (XWINMMR 3.0). Two-dimensional INADEQUATE experiments[29] were performed with the Bruker pulse program inad using a 90° read pulse (8.0 μs). Further parameters were as follows: td2, 2k; ns, 64; d1, 2s, d4, 6ms; td1, 800; sw2, 150; sw1, 75 ppm; aq-mode, qsim; mc2, qf; wdw2, gm; lb2, −0.6; gm2, 0.02; wdw1, qsine; ssb1, 2.

The analysis of ^{13}C enrichment and isotopomer composition was performed as described.[23] Briefly, ^{13}C NMR spectra of isotope-labeled samples and of samples with natural ^{13}C abundance were recorded under the same experimental conditions. Integrals were determined for every ^{13}C NMR signal, and the signal integral for each respective carbon atom in the labeled compound was referenced to that of the natural abundance material, thus affording relative ^{13}C abundances for each position in the labeled molecular species. Absolute ^{13}C abundances of **2** were obtained via normalization of the relative values to 1.1% ^{13}C of the methyl group of the 2-acetyl moiety (C-37), which was derived from acetyl chloride with natural ^{13}C abundance (i.e., 1.1% ^{13}C abundance). For hyperforin, relative ^{13}C abundances were normalized to a value of 1.5% for C-10, which has been accurately determined in the 2-acetyl derivative.

In NMR spectra of multiple-labeled samples displaying ^{13}C−^{13}C couplings, each satellite in the ^{13}C NMR spectra was integrated separately. The relative fractions of each respective satellite pair (corresponding to a certain coupling pattern, cf. Figure 6 and Table 1) in the total signal integral of a given carbon atom were calculated (% ^{13}C−^{13}C in Table 1). Relative isotopomer abundances were then referenced to the global absolute ^{13}C abundance for each carbon atom (shown as mol % in Figure 6).

Supporting Information Available: ^{1}H and ^{13}C NMR assignments of **1** and **2**. Chemical shifts and coupling constants and observed NMR connectivities by two-dimensional HMBC, NOESY, COSY, and INADEQUATE experiments. Parts of two-dimensional NOESY and HMBC spectra. This material is available free of charge via the Internet at http://pubs.acs.org.

References

(1) Erdelmeier, C. A. J. Hyperforin, possibly the major non-nitrogenous secondary metabolite of *Hypericum perforatum L. Pharmacopsychiatry* **1998**, *31*, 2−6.

(2) Whooley, M. A.; Simon, G. E. Managing depression in medical outpatients. *New Engl. J. Med.* **2001**, *343*, 1942−1950.

(3) Chatterjee, S. S.; Bhattacharya, S. K.; Wonneman, M.; Singer, A.; Müller, W. E. Hyperforin as a possible antidepressant component of hypericum extract. *Life Sci.* **1998**, *63*, 499−510.

(4) Müller, W. E.; Singer, A.; Wonneman, M.; Hofner, U.; Rolli, M.; Schäfer, C. Hyperforin represents the neurotransmitter reuptake inhibiting constituent of hypericum extract. *Pharmacopsychiatry* **1998**, *31* (Suppl. I), 16−21.

(5) DiCarlo, G.; Borrelli, F.; Ernst, E.; Izzo, A. A. St. John's Wort: Prozac from the plant kingdom. *Trends Pharmacol. Sci.* **2001**, *22*, 292−297.

(6) Kaehler, S. T.; Sinner, C.; Chatterjee, S. S.; Philippa, A. Hyperforin enhances the extracellular concentrations of catecholamines, serotonin and glutamate in the rat locus coeruleus. *Neurosci. Lett.* **1999**, *262*, 199−202.

(7) Gurevich, A. I.; Dobrynin, V. N.; Kolosov, M. N. Popravko, S. A.; Riabova, I. D. Antibiotic hyperforin from *Hypericum perforatum L. Antibiot. Khimioter.* **1971**, *16*, 510−513.

(8) Schempp, C. M.; Kirkin, V.; Simon-Haarhaus, B.; Kersten, A.; Kiss, J.; Termeer, C. C.; Gilb, B.; Kaufmann, T.; Borner, C.; Sleeman, J. P.; Simon, J. C. Inhibition of tumor cell growth by hyperforin, a novel anticancer drug from St. John's wort that acts by induction of apoptosis. *Oncogene* **2002**, *21*, 1242−1250.

(9) Schempp, C. M.; Pelz, K.; Wittmer, A.; Schöpf, E.; Simon, J. C. Antibacterial activity of hyperforin from St. John's wort, against multiresistant *Staphylococcus aureus* and gram-positive bacteria. *Lancet* **1999**, *19*, 353.

(10) Moore, L. B.; Goodwin, B.; Stones, S. A.; Wisely, G. B.; Serabjit-Singh, C. J.; Willson, T. M.; Collins, J. L.; Kliewer, S. A. St. John's wort induces hepatic drug metabolism through activation of the pregnane X receptor. *Proc. Natl. Acad. Sci. U.S.A.* **2000**, *97*, 13, 7500−7502.

(11) Perloff, M. D.; Moltke, L. L.; Stormer, E.; Shader, E.; Greenblatt, D. J. Saint John's Wort: an in vitro analysis of P-glycoprotein induction due to extended exposure. *Br. J. Pharmacol.* **2001**, *134*, 1601−1608.

(12) Obach, R. S. Inhibition of Human Cytochrome P 450 Enzymes by constituents of St. John's Wort, an herbal preparation used in treatment of depression. *Pharmacol. Exp. Ther.* **2000**, *294*, 88−95.

(13) Vogel, G. Pharmacology: How the body's garbage disposal may inactivate drugs. *Science* **2001**, *291*, 35−37.

(14) Bystrov, N. S.; Chernov, B. K.; Dobrynin, V.-N.; Kolosov, M. N. The structure of hyperforin. *Tetrahedron Lett.* **1975**, *16*, 2791−2794.

(15) Brondz, I.; Greibrokk, T.; Groth, P. A.; Aasen, A. J. The relative stereochemistry of hyperforin − an antibiotic from *Hypericum perforatum L. Tetrahedron Lett.* **1982**, *23*, 1299−1300.

(16) Brondz, I.; Greibrokk, T.; Groth, P. A.; Aasen, A. J. The absolute configuration of hyperforin, an antibiotic from *Hypericum perforatum L.,* based on the crystal structure determination of its *p*-bromobenzoate ester. *Acta Chem. Scand. A* **1983**, *37*, 263−265.

(17) Eisenreich, W.; Rohdich, F.; Bacher, A. Deoxyxylulose phosphate pathway to terpenoids. *Trends Plant Sci.* **2001**, *6*, 78−84.

(18) Bilia, A. R.; Bergozzi, M. C.; Mazzi, G.; Vincieri, F. F. Analysis of plant complex matrixes by use of nuclear magnetic resonance spectroscopy: St. John's wort extract. *J. Agric. Food Chem.* **2001**, *49*, 2115−2124.

(19) Orth, H. C. J.; Rentel, C.; Schmidt, P. C. Isolation, purity analysis and stability of hyperforin as a standard material from *Hypericum perforatum* L. *J. Pharm. Pharmacol.* **1999**, *51*, 193−200.

(20) Margl, L.; Eisenreich, W.; Adam, P.; Bacher, A.; Zenk, M. H. Biosynthesis of thiophenes in *Tagetes patula. Phytochemistry* **2001**, *58*, 875−881.

(21) Eichinger, D.; Bacher, A.; Zenk, M. H.; Eisenreich, W. Analysis of metabolic pathways via quantitative prediction of isotope labeling patterns: a retrobiosynthetic ^{13}C NMR study on the monoterpene loganin. *Phytochemistry* **1999**, *51*, 223−236.

(22) Bacher, A.; Rieder, C.; Eichinger, D.; Arigoni, D.; Fuchs, G.; Eisenreich, W. Elucidation of novel biosynthetic pathways and metabolite flux patterns by retrobiosynthetic analysis. *FEMS Microbiol. Rev.* **1999**, *22567*−22589.

(23) Eisenreich, W.; Bacher, A. Elucidation of biosynthetic pathways by retrodictive/predictive comparison of isotopomer patterns determined by NMR spectroscopy. In *Genetic Engineering, Principles and Methods*; Setlow, J. K., Ed.; Kluwer Academic/Plenum Publishers: 2000; Vol. 22, pp 121−151.

(24) Goese, M.; Kammhuber, K.; Bacher, A.; Zenk, M. K.; Eisenreich, W. Biosynthesis of bitter acids in hops. A ^{13}C NMR and ^{2}H NMR study on the building blocks of humulone. *Eur. J. Biochem.* **1999**, *263*, 447−454.

(25) Glawischnig, E.; Tomas, A.; Eisenreich, W.; Spiteller, P.; Bacher, A.; Gierl, A. Auxin biosynthesis in maize kernels. *Plant Physiol.* **2000**, *123*, 1109−1119.

(26) Wang, C.-Z.; Maier, U. H.; Eisenreich, W.; Adam, P.; Obersteiner, I.; Keil, M.; Bacher, A.; Zenk, M. H. Unexpected biosynthetic precursors of amarogentin − a retrobiosynthetic ^{13}C NMR study. *Eur. J. Org. Chem.* **2001**, 1459−1465.

(27) Werner, I.; Bacher A.; Eisenreich, W. Retrobiosynthetic NMR studies with ^{13}C-labeled glucose. Formation of gallic acid in plants and fungi. *J. Biol. Chem.* **1997**, *272*, 25474−25482.

(28) Crout, D. H. G.; Hedgecock, C. J. R.; Lipscomb, E. L.; Armstrong, F. B. Stereochemistry of valine biosynthesis. *Eur. J. Biochem.* **1980**, *110*, 439−444.

(29) Bax, A.; Freeman, R.; Frenkiel, T. A. An NMR technique for tracing out the carbon skeleton of an organic molecule. *J. Am. Chem. Soc.* **1981**, *103*, 2102−2104.